Title

Multiscale Modeling of Power Plant Performance Enhancement Utilizing Asynchronous Cooling With Thermal Energy Storage

Journal

Journal of Heat Transfer, 142(5)

ISSN

0022-1481

Authors

Gagnon, Lauren
Helmns, Dre
Carey, Van P

Publication Date

2020-05-01

DOI

10.1115/1.4046773

Peer reviewed

Lauren Gagnon[1]
Department of Mechanical Engineering,
University of California,
5117 Etcheverry Hall,
2505 Hearst Avenue,
Berkeley, CA 94709
e-mail: lauren_gagnon@berkeley.edu

Dre Helmns
Department of Mechanical Engineering,
University of California,
5117 Etcheverry Hall,
2505 Hearst Avenue,
Berkeley, CA 94720
e-mail: drehelmns@lbl.gov

Van P. Carey
Department of Mechanical Engineering,
University of California,
5117 Etcheverry Hall,
2505 Hearst Avenue,
Berkeley, CA 94709
e-mail: vpcarey@berkeley.edu

Multiscale Modeling of Power Plant Performance Enhancement Utilizing Asynchronous Cooling With Thermal Energy Storage

This study links a model of thermal energy storage (TES) performance to a subsystem model with heat exchangers that cool down the storage at night; this cool storage is used to precool the air flow for a power plant air-cooled condenser during peak day temperatures. The subsystem model is also computationally linked to a model of Rankine cycle power plant performance to predict additional power the plant could generate due to the additional cooling. The model was used to explore the effects of varying phase change material (PCM) melt temperature and the energy input and rejection control settings with the goal of maximizing efficiency for a 50 MW power plant operating in the desert regions of Nevada for an average summer day. The results suggest that the kWh output of the modeled plant can be increased by up to 3.25% during the heat input/cold extraction period, and a cost analysis estimates that the TES system has the potential to provide additional revenue of up to $686,000 per year, depending on electricity cost and parameter choices. [DOI: 10.1115/1.4046773]

Introduction

Motivation. The motivation behind this research was to improve the efficiency of Rankine power plants with air-cooled steam condensers in order to reduce the high volume of water usage at power plants. Traditionally, steam produced by thermoelectric power plants is cooled by directing it over an array of pipes filled with cold water, which causes the steam to condense. This process is highly water intensive and uses between 730 and 830 gal/MWh [1], proving it to be an impractical cooling method in areas where water conservation is an issue. Air-cooled steam condenser power plants do exist, but the air is not always at an ideal temperature for air-cooling to be efficient. However, augmented cooling via thermal energy storage (TES) of phase change material (PCM) can increase the efficiency of power or refrigeration cycles [2] with the potential to increase power plant efficiency up to 60% with the addition of heat recovery systems [3]. Therefore, to improve power plant efficiency, this study has conducted research to show proof of concept air-*precooling* technology using latent thermal energy storage that employs phase change material.

Prior and Current Work. Latent heat TES systems using PCMs other than water have been around since the 1980s with applications ranging from building to power plant cooling [4]. However, prior to this work, no research had been done to assess and quantify the performance of TES air-precooling technology in full-scale power plants or with the implementation of practical conditions. Earlier analyses of phase change thermal storage performance have generally modeled specific details of heat transfer in the storage unit structure with constant boundary conditions, thereby neglecting interaction in a subsystem.

For example, El-Dessouky and Al-Juwayhel [5] use a second law analysis to characterize the TES by entropy generation numbers. While this study analyzed an entire transient melting and freezing cycle, the PCM remained at the melt temperature throughout. Similarly, Ismail and Goncalves [6] explored a two-dimensional model of a tube immersed in PCM applying a constant inlet boundary condition without discussing the heat exchanger that might supply this input. Alkilani et al. [7] conducted a theoretical investigation of output air temperature of an indoor heater which utilizes a PCM heat exchanger. In this model, the PCM was used to store solar heat from throughout the day that could then be used to provide heating at night. This model implemented only a constant input air temperature to the PCM heat exchanger, thereby neglecting the inevitable changes in the room's temperature. Of the few analyses that have considered a variable inlet air temperature, such as the one produced by Vakilaltojjar and Saman [8], a simple scheme consisting only of a PCM heat exchanger was examined, whereas the subsystem considered by this analysis includes external heat exchangers which govern the temperature of the working fluid within the PCM heat exchanger.

This paper builds upon previous work by Dre Helmns and Van P. Carey to model a 24-hour cycle operation of a TES subsystem connected to a Rankine cycle power plant [9]. This research differs from Helmns and Carey's model, however, in that it incorporates realistic temporally transient ambient temperature data and determines metrics for assessing and quantifying the improvement to the power plant's production. Furthermore, Helmns and Carey's work neither explores the optimization of the TES subsystem nor the financial payback period associated with the implementation of such technology, while these analyses were conducted for this study.

Multiscale Modeling of Thermal Energy Storage and External Heat Exchanger Subsystem

The proposed TES and heat exchanger subsystem examined in Helmns and Carey's model has the goal of increasing the efficiency of the steam condensing process in air-cooled power plants. The improved efficiency of this process results in an increase in the net power produced by the power plant facilitated by decreasing the low system temperature within the Rankine power cycle.

[1]Corresponding author.

Contributed by the Heat Transfer Division of ASME for publication in the Journal of Heat Transfer. Manuscript received May 14, 2019; final manuscript received March 2, 2020; published online April 10, 2020. Assoc. Editor: Amitabh Narain.

The setup of the TES and heat exchanger subsystem, which allows for precooling of the air flow sent into the steam condenser, is shown in Fig. 1. The left side of Fig. 1 shows the TES device, comprising a PCM matrix that consists of phase change material (the smaller, vertical sections), aluminum mesh and structural fins (the lines separating each section), and flow channels containing a working fluid (the horizontal channels). The working fluid that passes through the TES also passes through an adjacent external heat exchanger in a closed-loop, also shown in the left side of Fig. 1. The right side of Fig. 1 illustrates how this external heat exchanger can be operated in one of two configurations. Both configurations depict an external heat exchanger with an open loop of working fluid, paired with a TES device connected via a closed-loop that circulates through the heat exchanger. The configuration labeled "a" shows the closed-loop working fluid absorbing heat from the open-loop working fluid and transferring it to the PCM, while the configuration labeled "b" shows the closed-loop working fluid absorbing heat from the PCM and transferring it to the open-loop working fluid.

The two configurations depicted on the right side of Fig. 1 are necessary for the proposed asynchronous operation of the TES and external heat exchanger subsystem. The implementation of the subsystem into a Rankine cycle power plant is schematically shown in Fig. 2, where the four quadrants correspond to the four processes the TES goes through to achieve its asynchronous functionality. The first process, shown in the upper-left box, is precooling or extraction, where it is preferable to begin with a completely frozen PCM. During this phase, hot air ($T_{\text{source,in}}$) flows from the ambient surroundings ($\dot{m}_{\text{source}} > 0$) and is chilled by sending it through the air precooler to deliver its heat to the closed-loop fluid entering the TES. The closed-loop fluid is then chilled by rejecting heat to the cold storage matrix and melting the PCM. Now cooler, the closed-loop fluid, is able to precool the air in the open loop ($T_{\text{source,out}}$) before it enters the steam condenser. In other words, while the surrounding ambient air is warmer than the PCM, the TES and external heat exchanger subsystem is used to precool the air before it is then used to condense steam as part of the Rankine cycle.

The second process, shown in the upper-right box, is a quiescent storage period, during which no flow occurs in the TES ($\dot{m}_{\text{closed}} = 0$), and air is taken into the steam condenser from the ambient through a bypass door. These periods are strategically designed to occur when the ambient air temperature is very close to the melting temperature of the PCM ($T_{\text{m}} \pm T_{\text{thresh}}$), as little to no advantage would be gained from operating the TES and external heat exchanger subsystem during this time.

The third process, shown in the lower-right box, is night cooling or charging. During this period, cool air ($T_{\text{sink,in}}$) flows from the ambient surroundings ($\dot{m}_{\text{sink}} > 0$) through the heat exchanger to cool the counterflowing working fluid entering the TES unit. Provided that the temperature of the fluid entering the TES device is less than the PCM melt temperature, the PCM will undergo freezing. In other words, while the surrounding ambient air is cooler than the PCM, that air is used to cool down and freeze the PCM within the TES to prepare it for the eventual next extraction phase. The fourth and final process, shown in the lower-left box, is a second quiescent storage period, after which the cycle begins again.

The model utilized in this study was developed by Helmns and Carey [9]. Helmns and Carey's model is similar to that of a compact heat exchanger but considers a transient process in which a PCM either stores or rejects heat through latent heat transfer while phase change is occurring. The focus of Helmns and Carey's analysis is on a unit cell of one long passage, as shown in Fig. 3, with the mass flowrate per passage designated as $\dot{m}_{\text{closed}}$. The unit cell, of length dz, is composed of the working fluid flow passage and the surrounding PCM section. This element includes the tube wall, fin structures, and mesh, which conduct heat into the PCM.

To derive the governing equations in Helmns and Carey's model, the TES unit cell is divided into two control volumes: one around a differential element of PCM matrix and another around a differential section of the flow passage. Conservation of energy is applied to each, as shown in Eqs. (1) and (2). Equation (1) represents the transient exchange of sensible energy between the working fluid and the PCM, and Eq. (2) dictates the transient exchange of latent energy between the working fluid and the PCM that leads to melting or freezing. In doing so, Eq. (2) calculates the melt fraction of the PCM, x_{e}, which is a result of interest in this paper. To account for the energy exchange across the flow channel wall, conservation of energy on the second control volume around the working fluid of the unit cell was also applied, as shown in Eq. (3). Equation (3) describes how energy is advected along the working fluid channel as well as exchanged with the storage element throughout the passage.

For $T_{\text{e}} \neq T_{\text{m}}$ and $x_{\text{e}} = 0$ or $x_{\text{e}} = 1$

$$\frac{\partial T_{\text{e}}}{\partial t} = \frac{U_{\text{closed}} s_{\text{w}}}{\bar{\rho}_{\text{e}} \bar{c}_{\text{pe}} \nu'} (T_{\text{closed}} - T_{\text{e}}); \quad \frac{\partial x_{\text{e}}}{\partial t} = 0 \tag{1}$$

For $T_{\text{e}} = T_{\text{m}}$ and $0 < x_{\text{e}} < 1$

$$\frac{\partial x_{\text{e}}}{\partial t} = \frac{U_{\text{closed}} s_{\text{w}}}{\bar{\rho}_{\text{e}} h_{\text{ls}} \nu'} (T_{\text{closed}} - T_{\text{e}}); \quad \frac{\partial T_{\text{e}}}{\partial t} = 0 \tag{2}$$

For all T_{e} and x_{e}

$$\frac{\partial T_{\text{closed}}}{\partial t} = -\left(\frac{\dot{m}_{\text{closed}}}{\rho_{\text{cl}} A_{\text{c}}}\right) \frac{\partial T_{\text{closed}}}{\partial z} + \frac{U_{\text{closed}} s_{\text{w}}}{\rho_{\text{cl}} A_{\text{c}} c_{\text{p,cl}}} (T_{\text{e}} - T_{\text{closed}}) \tag{3}$$

Building off Eqs. (1)–(3), subsequent equations that are derived in Helmns and Carey's model produce the other results of interest in this paper. Equations (4) and (5) calculate the output air temperatures from both the precooler, $T_{\text{source,out}}$, and the night cooler, $T_{\text{sink,out}}$, respectively. The outlet temperatures from the TES

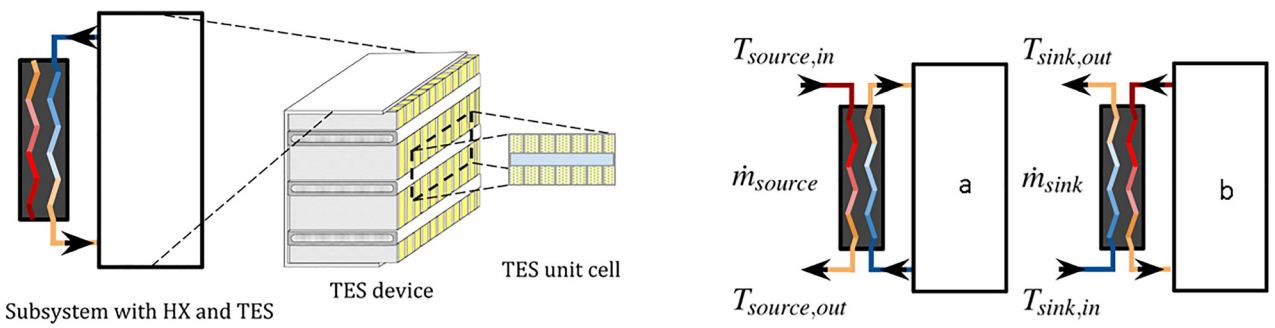

Fig. 1 (left) Schematic depicting TES (PCM, fins, mesh, and flow passage) and external heat exchanger subsystem and (right) TES coupled with external heat exchanger for heat storage (*a*) and heat off-loading (*b*)

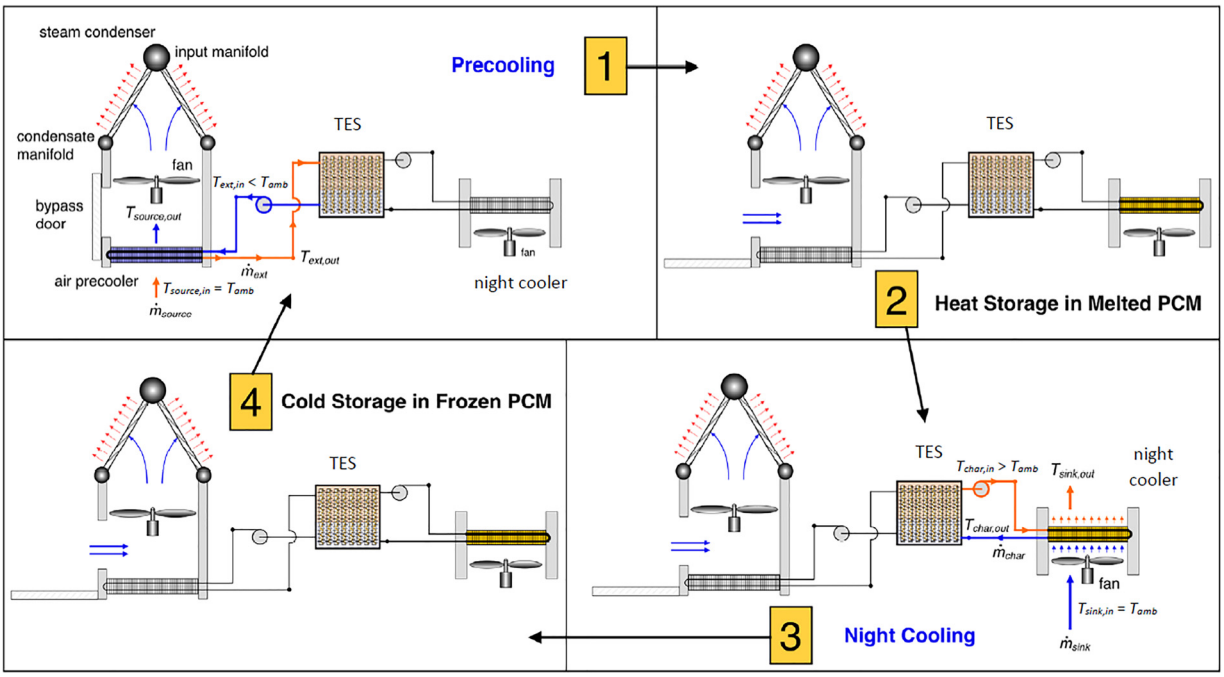

Fig. 2 Case study cycle consisting of precooling, first storage phase, night cooling, and second storage phase

during extraction, $T_{ext,in}$, and charging, $T_{char,in}$, are calculated when solving Eqs. (1)–(3), and $T_{source,in}$ and $T_{sink,in}$ are the ambient air temperatures during extraction and charging, respectively,

$$T_{source,out} = \varepsilon_{so}\frac{\dot{m}_{ext}c_{p,cl}}{\dot{m}_{so}c_{p,op}}T_{ext,in} + \left(1 - \varepsilon_{so}\frac{\dot{m}_{ext}c_{p,cl}}{\dot{m}_{so}c_{p,op}}\right)T_{so,in} \quad (4)$$

$$T_{sink,out} = \varepsilon_{si}\frac{\dot{m}_{char}c_{p,cl}}{\dot{m}_{si}c_{p,op}}T_{ch,in} + \left(1 - \varepsilon_{si}\frac{\dot{m}_{char}c_{p,cl}}{\dot{m}_{si}c_{p,op}}\right)T_{si,in} \quad (5)$$

Further details of Helmns and Carey's model can be found in previous publications [9]. In addition, the overall heat transfer coefficient between the bulk working fluid and PCM matrix element, U_{closed}, used in Eqs. (1)–(3), can be calculated using several different models, all of which are applicable within Helmns and Carey's model. For a detailed explanation and description of the method used in the model to calculate the overall heat transfer coefficient in this study, see Ref. [10]. If other methods for calculating this value are desired, see Ref. [11].

Implementation of Thermal Energy Storage and External Heat Exchanger Subsystem Into Power Plant

To explore a subsystem that models realistic operating conditions for TES, a moderate Rankine power plant with a capacity, $\dot{W}$, of 50 MW with an assumed constant thermal efficiency, η_{cyc}, of 0.3073, was analyzed. The steam condenser within this Rankine power plant was assumed to have an effectiveness of 0.80 and an operating temperature of 50.8 °C. The heat transfer rate within the steam condenser, $\dot{Q}_{sc}$, for the selected power plant size and thermal efficiency was calculated to be 112.7 MW from Eq. (6).

$$\dot{Q}_{sc} = \dot{W}\left(\frac{1 - \eta_{cyc}}{\eta_{cyc}}\right) \quad (6)$$

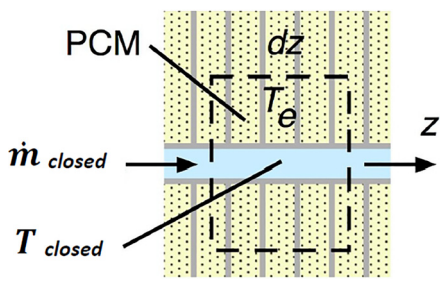

Fig. 3 TES unit cell including control volume around differential element of PCM matrix and differential section of flow passage

Inputs to Multiscale Model. To solve Eqs. (1)–(3), the geometry of the TES structure, shown in Table 1, was selected based on a prototype designed by project collaborator Dr. Jianping Tu of Allcomp with input from Boeing. Regarding the external heat exchangers, both the values of the effectiveness of the precooler, ε_{source}, and the night cooler, ε_{sink}, were assumed to be 0.80 with the goal of reaching 0.95 effectiveness in the TES; however, effectiveness values of 0.85 or higher were accepted. The open- and closed-loop working fluids in the external heat exchangers were taken as the ambient air and a one to one mixture of ethylene glycol and water (EGW 50/50), respectively. The PCM utilized by the model in this analysis was a specific variant of lithium nitrate trihydrate (LNT), $LiNO_3{\cdot}3H_2O$, which made possible the use of a melt temperature of 30 °C [12]. For the model, the density, ρ_{PCM}, and latent heat of fusion, h_{ls}, of LNT were taken to be 1462.5 kg/m^3 and 278.14 kJ/kg, respectively.

To determine the ambient air input for the model, Las Vegas, NV, was selected as the location from which to gather weather data because it lies in a drought-stricken desert region less than 50 miles away from the Walter Higgins Generating Station, a power plant that currently uses air-cooling technology and could greatly

Table 1 TES case study dimensional variables—flow passage geometry

Wetted perimeter of flow passage	s_w	0.0942000	m
Length of flow passage	L	0.4070000	m
Cross-sectional area of flow passage	A_c	0.0000897	m^2
PCM matrix volume per unit flow length	v'	0.0001993	m^2

benefit from the TES precooling subsystem assessed in this study. Hourly weather data from January 2013 through December 2017 was obtained from the Las Vegas Henderson Airport Weather Station (WBAN 53127) through use of the Local Climatological Data Tool on the National Oceanic and Atmospheric Administration (NOAA) website [13]. The months with temperatures above the specified PCM melt temperature of 30 °C were determined, as shown in Fig. 4.

It was found that June through August had over 2000 h recorded above the 30 °C threshold for the 5 years surveyed. May and September also had a moderate number of hours recorded above 30 °C during this time. Therefore, from approximately the last third of May through the first half of September, a total of about 4 months, it was assumed that the TES and external heat exchanger subsystem would be operable.

For this analysis, it was decided that one month from the four identified would be examined in detail and used as representative for the time the TES and external heat exchanger subsystem was assumed to be operable. The temperature fluctuations throughout an average day of each month were found by averaging the hourly temperature data of each day in the five year dataset. The left side of Fig. 5 shows the resulting average hourly temperature trends over 24-hour periods in May (only after the 20th), June, July, August, and September (only before the 15th).

August's peak temperature on an average day falls in the middle of the group with peak temperatures close to those on an average day of June or July. Thus, August was selected as the representative month. It was decided that an average daily temperature curve would be most representative of typical August weather, and this choice was later validated with a sensitivity analysis showing that the TES and external heat exchanger subsystem could operate under a variety of conditions. To prepare August's average daily temperature curve to be an input to the model, the curve on the right side of Fig. 5 was produced. To create this curve, the timeline of August's average temperature curve was shifted such that the first timestamp corresponded to a time of day with a temperature above the melting temperature of the PCM, and a polynomial function was fit to the resulting curve. Based on this curve, a temperature threshold of ±0.8 °C of the PCM melt temperature was selected, and it was determined that extraction could be supported for 12 h.

Scaling to Full-Sized Power Plant. To scale to the desired TES volume for a full-sized power plant from Helmns and Carey's unit cell analysis, the number of flow passages, n_{chan}, within the TES was determined based on the desired duration of extraction, in this case 12 h, in conjunction with a working fluid mass flowrate within those channels that allowed for the PCM to reach the desired target melt fraction of 0.95 by the end of the extraction period. Once the number of flow passages was selected in this manner, in this case corresponding to a TES volume of 1772 m^3 from Eq. (7), the analysis from Helmns and Carey's model that was performed on one flow passage was applied to the others.

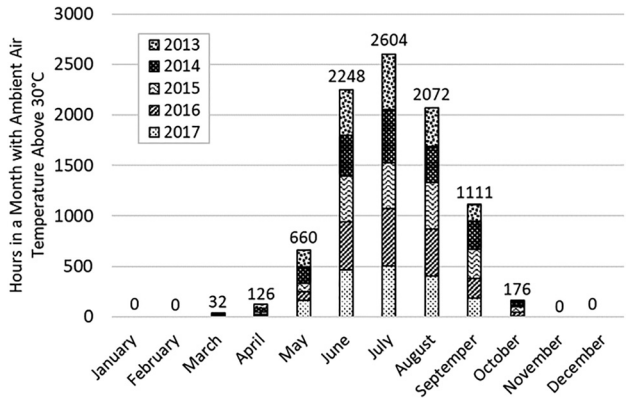

Fig. 4 Hours by month in which ambient air temperature exceeded 30 °C for Las Vegas, NV, from 2013 to 2017

$$V_{TES} = L\left[A_c n_{chan} + \nu'(n_{chan} - 1)\right] \tag{7}$$

Results and Discussion

The model results from using the average August ambient temperature curve, as well as the other discussed inputs, can be seen in Fig. 6. This plot shows the open-loop air temperatures at the inlet and outlet of the precooler throughout extraction, depicted as solid and dashed curves within the precooling region, respectively. The open-loop air temperatures at the inlet and outlet of the night cooler throughout charging are depicted as solid and dashed curves within the night cooling region, respectively, and the PCM melt fraction is depicted as a solid curve throughout the entire process.

In this plot, the PCM melt fraction achieves the goal of reaching 0.95 just at the end of extraction and 0.05 just at the end of charging. Figure 6 also shows that at peak ambient temperatures during extraction, the precooling process decreased the air inlet temperature into the precooler by about 6 °C (ΔT_{source}) by the time it reached the outlet, thus decreasing the low system temperature by this amount, which greatly improved the efficiency of the power plant.

Efficiency Metrics. To quantify the efficiency improvement due to the implementation of the TES and external heat exchanger subsystem, the variable power output throughout a 24-hour production period was calculated, as shown in the following equations:

$$\eta_{cyc,var} = 0.6\left(1 - \frac{T_{source,out}}{T_{boiler}}\right) \tag{8}$$

$$\dot{W}_{var} = \dot{Q}_{sc}\left(\frac{\eta_{cyc,var}}{1 - \eta_{cyc,var}}\right) \tag{9}$$

where the Rankine efficiency, $\eta_{cyc,var}$, is assumed to be 60% of the Carnot efficiency, and T_{boiler} is the boiler temperature, which throughout this study was assumed to be 362.4 °C. Because the temperature output from the precooler, $T_{source,out}$, varied throughout the day, the efficiency of the Rankine cycle, and therefore the power output, $\dot{W}_{var}$, varied throughout the day as well, as shown in Fig. 7.

To further assess the improvement in the power produced by the implementation of the TES and external heat exchanger subsystem, two other metrics were evaluated: the percent increase in energy generation throughout extraction, e_{ext}, or over a 24-hour period, e_{day}, due to the subsystem implementation. To determine these percentages, the energy generated by the power plant was calculated by integrating the power production during the time windows of interest, as shown in the following equation:

$$E_{plant} = \int_{t_1}^{t_2} \dot{W}_{var} dt \tag{10}$$

where for the energy generation throughout extraction, E_{ext}, $t_1 = 0$ and $t_2 = t_{ext}$, and for the energy generation after extraction and throughout the rest of the day, E_{day}, $t_1 = t_{ext}$ and $t_2 = 24$ h. The energy generation during what would have been the extraction period but if the precooling process did not take place, $E_{no\ ext}$, was calculated using Eq. (10) as well. The difference between E_{ext} and $E_{no\ ext}$ was then defined as ΔE_{ext}. Finally, e_{ext} and e_{day} were calculated using Eq. (11),

$$e_{plant} = \frac{\Delta E_{ext}}{E_{other}} \tag{11}$$

where for e_{ext}, E_{other} is $E_{no\ ext}$, and for e_{day}, E_{other} is $E_{no\ ext}$ added to E_{day}.

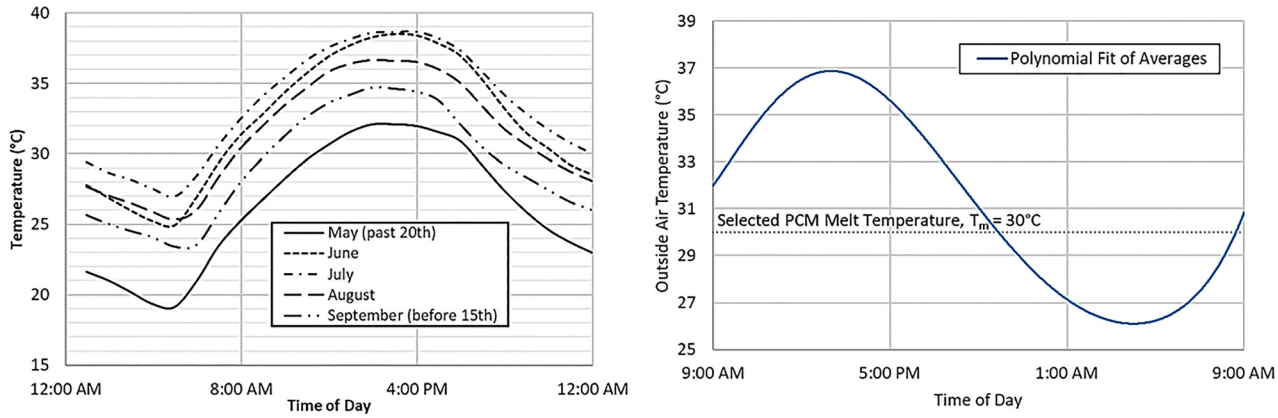

Fig. 5 (left) Average hourly Las Vegas, NV, temperature data for May, June, July, August, and September averaged from 2013 to 2017 and (right) approximate polynomial curve for outside air temperature throughout an average August day in Las Vegas, NV

To better visualize these percentages, Fig. 7 can be referenced, where e_{ext} is the area between the two curves divided by the area under the lower curve from $t = 0$ to t_{ext}, and e_{day} is the area between the two curves divided by the entire area under the lower curve. These results and other relative inputs and outputs for this case are shown in Table 2. With energy generation during extraction increased by 10.4 MWh, corresponding to e_{ext} and e_{day} figures of 1.70% and 0.85%, respectively, these results quantitatively illustrate the potential benefits in production available to power plants with air-cooled steam condensers through implementation of the TES and external heat exchanger subsystem.

Thermal Energy Storage Volume Adjustment, Extraction Time Optimization, and Sensitivity Analysis. As mentioned previously, this first test case utilized an extraction period of 12 h, which was selected because it was the longest length of extraction supported by the ambient temperature conditions in Las Vegas on an average day of August. However, the longest possible extraction time was not guaranteed to be the most beneficial to the plant; therefore, the extraction time of the subsystem was varied by adjusting the upper temperature threshold in conjunction with the number of flow passage channels and the total mass flowrate in the TES.

The left side of Fig. 8 shows the relationship between the percent increase in energy generation over a 24-hour period and the volume of the TES as the number of flow passage channels, and therefore extraction time, changes. These data demonstrate a very clear, positive trend between the two variables. Contrarily, the right side of Fig. 8 shows the relationship between the percent increase in energy generation throughout the extraction period and the volume of the TES, which displays a negative trend, suggesting that there are diminishing returns for implementing larger TES volumes and correspondingly longer extraction times. To determine an appropriate total TES volume, both energy percentage metrics were normalized by their respective maximums and compared directly with one another, as shown on the left side of Fig. 9.

Using the intersection point seen on the left side of Fig. 9, a total TES volume of about 1500 m^3 was selected, as it balances both e_{ext} and e_{day}. From here, the extraction time was determined to be 8.7 h based on the relationship seen on the right side of Fig. 9. Using this optimized extraction time, the energy generation of the plant increased by 9.0 MWh, corresponding to e_{ext} and e_{day} values of 2.06% and 0.73%, respectively, as shown in Table 3.

As previously mentioned, it was desired to confirm that selecting an average daily August temperature curve was a valid input into the model. As such, a sensitivity analysis was performed in which a characteristically hot 24-hour temperature curve for August as well as a characteristically cool 24-hour temperature curve for August were input into the optimized model and compared with the results from the average daily August temperature curve. A comparison of the three temperature curves is shown in Fig. 10.

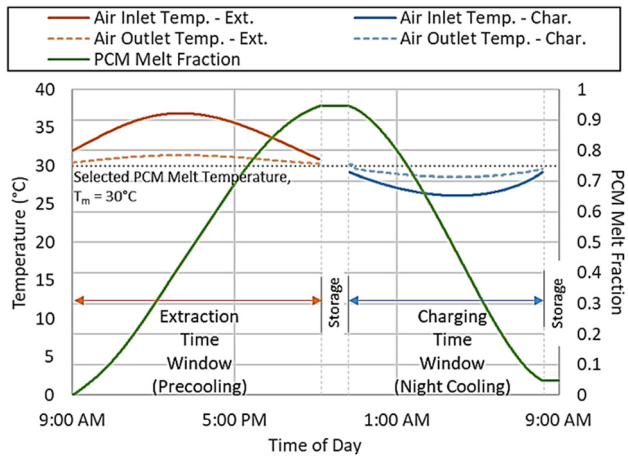

Fig. 6 Melt fraction of PCM and air inlet and outlet temperatures to and from TES for extraction (12 h) and charging versus time of day in Las Vegas, NV, for average day in August

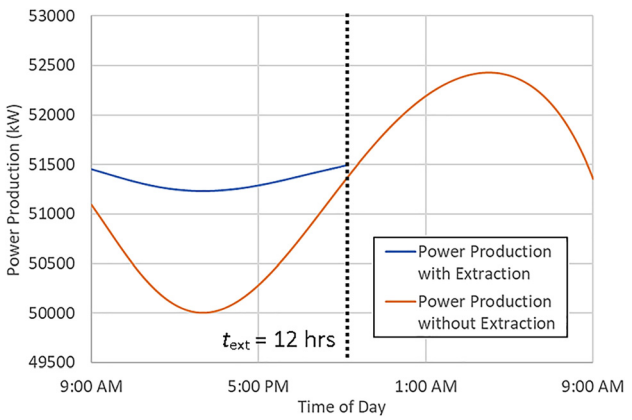

Fig. 7 Power production fluctuation with and without precooling process for 50 MW power plant during an average August day in Las Vegas, NV, for $T_m = 30\,^{\circ}C$

Table 2 (left) Inputs and (right) outputs from August model for TES and external heat exchangers subsystem in Las Vegas for $T_m = 30\,^{\circ}C$ and extraction time of approx. 12 h

T_m (°C)	t_{ext} (h)	V_{TES} (m^3)	T_{up} (°C)	T_{low} (°C)	ΔE_{ext} (MWh)	ΔE_{ext} (MJ)	e_{ext} (%)	e_{day} (%)	ΔT_{source} (°C)
30	12	1772	30.8	29.2	10.4	37,440	1.70	0.85	5.5

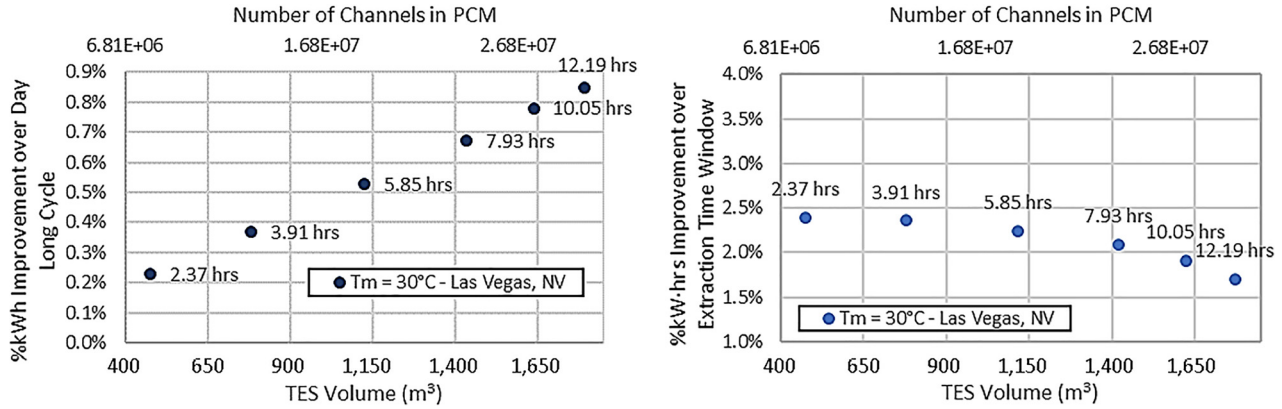

Fig. 8 (left) %kWh gained throughout day for different lengths of extraction periods and (right) %kWh gained throughout extraction time for different lengths of extraction periods versus TES volume for average day in August

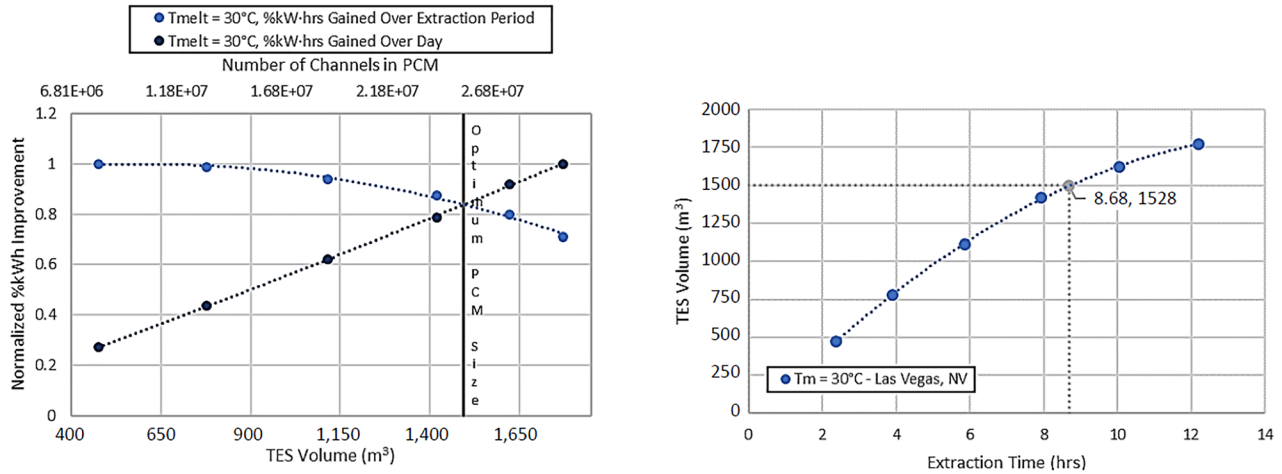

Fig. 9 (left) Normalized %kWh gained throughout extraction period and %kWh gained throughout day versus TES volume and (right) minimum required channels for 95% effectiveness (melting) versus extraction time for average day in August

Table 3 (left) Inputs and (right) outputs from August model for TES and external heat exchangers subsystem in Las Vegas for $T_m = 30\,^{\circ}C$ and extraction time of approximately 8.7 h

Day type	T_m (°C)	t_{ext} (h)	V_{TES} (m^3)	T_{up} (°C)	T_{low} (°C)	ΔE_{ext} (MWh)	ΔE_{ext} (MJ)	e_{ext} (%)	e_{day} (%)	ΔT_{source} (°C)
Avg.	30	8.7	1528	34.0	29.2	9.0	32,400	2.06	0.73	5.4
Hot	30	8.7	1528	38.0	29.2	17	60,800	3.81	1.40	9.4
Cool	30	8.7	1528	31.0	29.2	5.5	19,800	1.27	0.44	4.0

All things equal, other than adjusting the upper temperature threshold to ensure a constant extraction time, it was found that using the TES and external heat exchanger subsystem on a characteristically hot August day would increase the performance of the powerplant by 3.81% during the extraction period due to the large temperature differential between the outside air temperature and the cooling device. However, the temperature during this characteristically hot day did not become cool enough for the charging process to take place; therefore, the PCM would not refreeze on days such as these. Opposingly, on a characteristically cool August day, it was found that using the TES and external heat exchanger subsystem only increased the performance of the powerplant by 1.27% during extraction due to the relatively low temperature differential between the ambient air and the PCM. However, on days such as these, it is practically guaranteed that the PCM will completely refreeze during the charging phase. These results are shown in Table 3.

Overall, the subsystem proved to not be overly sensitive to differences in heightened or reduced ambient air temperature throughout a day. Additionally, due to the excess performance gains achieved during hotter days and the assured full charge of the PCM on cooler days, the positive outcomes observed on hotter

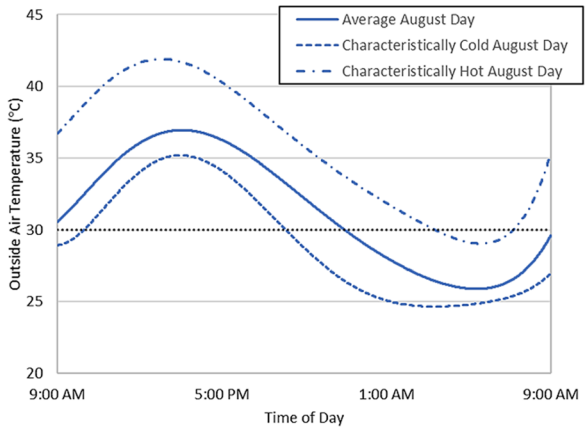

Fig. 10 Approximate polynomial curves for outside air temperature throughout an average August day, characteristically cool day, and characteristically hot day in Las Vegas, NV

days are balanced out by the less optimal outcomes observed on cooler days and vice versa. Due to the overall lack of sensitivity of the subsystem and the likelihood that there will be a balance of hotter and cooler days while operating the TES and external heat exchanger subsystem, it is believed that an average temperature curve was a valid input to the model to determine the feasibility and optimization of such a subsystem.

Effect of Phase Change Material Melt Temperature. Another parameter that was investigated to further improve the efficiency of the precooling process of the TES and external heat exchanger subsystem was the PCM melt temperature. To explore changing the PCM melt temperature, it was assumed that all other thermal properties of the PCM would remain the same as the original thermal properties used for LNT. Figure 11 shows the relationship between the percent increase in energy generation throughout the extraction period and total TES volume for various PCM melt temperatures, where the dotted vertical lines in this figure mark the optimized total TES volumes for each of the analyzed PCM melt temperatures. The inputs and outputs to and from the model for these cases are summarized in Table 4.

The trend shown in Fig. 11 indicates that as the PCM melt temperature is decreased, the same volume of TES can lead to greater percent increases in energy generation throughout the extraction period. However, it should be noted that the 28 °C PCM melt temperature case showed difficulties in achieving the desired PCM melt fraction for certain input configurations, and the 27 °C PCM melt temperature case had no input configurations that resulted in refreezing the PCM to the desired melt fraction. This inability to refreeze was due to the PCM melt temperature being pushed so low that nearly all ambient temperatures fell into the extraction

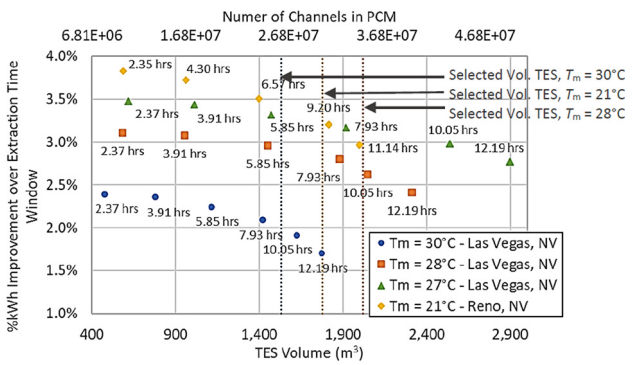

Fig. 11 %kWh gained throughout extraction time for different lengths of extraction periods versus TES volume for various PCM melting temperatures for average day in August

phase, leaving no time in the charging phase for refreezing to take place. Thus, a test case in Reno, NV, was explored, as shown in Fig. 11, due to Reno's similar desert environment, comparably warm daytime temperatures, and much cooler nighttime temperatures when likened to Las Vegas.

The same methods used for analyzing Las Vegas were used for analyzing Reno as well. Hourly weather data from January 2013 through December 2017 was obtained from the Reno Stead Airport Weather Station (WBAN 00279) through use of the Local Climatological Data Tool on the NOAA website [13]. August was again selected as the representative month, and the resulting average temperature curves can be seen in Fig. 12.

The results for this case, also found in Table 4, show that ΔE_{ext} was increased by 5.9 MW, corresponding to e_{ext} and e_{day} figures of 3.25% and 1.18%, respectively. These results suggest that using a PCM with a lower melt temperature can greatly increase the gains that are achieved in a Rankine power plant with an air-cooled steam condenser through the implementation of a TES and external heat exchanger subsystem.

Cost Analysis

A cost analysis was also performed to gain further insight regarding the benefit of implementing the subsystem. This cost analysis examined the three melt temperature cases that had been through the TES volume selection process and compared the investments required to implement these subsystems, the additional revenue they would produce, and the time required to pay off the investments using only the additional revenue produced by the subsystems for each of these cases. It should be noted that this cost analysis was limited to the TES device only and did not include an analysis of the external heat exchanges in the subsystem. This decision was made because the size and cost of the external heat exchanger are highly site dependent, making this expense difficult to estimate and thus considered to be outside the scope of this study. However, it is likely that the cost of the external heat exchanger would be negligible compared to the cost of the TES; therefore, leaving this expense out of the cost analysis was considered a reasonable approach.

To calculate the required investment for each of the three TES structures assessed in the Effect of Phase Change Material Melt Temperature section, a preliminary estimated price of $15.19 per MJ of storage available within the TES, C_{TES}, was provided by project collaborators at Boeing. Equation (12) was used to convert the TES volume to a storage capacity, E_{TES} [9]

$$E_{TES} = \rho_{PCM} \nu' L h_{ls} \varepsilon_{ext} (n_{chan} - 1) \tag{12}$$

Assuming the power plant would pay for the TES and external heat exchanger subsystem in full, the investment of the system was calculated using in the following equation:

$$C_{inv} = C_{TES} E_{TES} \tag{13}$$

Next, the annual profits produced by implementation of the TES and external heat exchanger subsystem, P_{annual}, were calculated using Eq. (14). In this equation, other than the excess energy generation produced by the plant through implementation of the subsystem, the local cost of electricity, C_{elec}, as well as the previously addressed assumption that the TES and external heat exchanger subsystem would only be in use a fraction of days per year, f, were taken into consideration

$$P_{annual} = \Delta E_{ext} f C_{elec} \tag{14}$$

For the analyzed cases, the subsystem was assumed to be operable for 4 months of the year, and the cost of electricity was found to be $0.11 per kWh in Las Vegas using the Southern Nevada residential single-family program [14] and $0.09 per kWh in Reno using the Northern Nevada domestic service program [15].

Table 4 (left) Inputs and (right) outputs to August model for TES and external heat exchanger subsystem in Las Vegas ($T_m = 30\,^\circ C$, $28\,^\circ C$, $27\,^\circ C$) and Reno ($T_m = 21\,^\circ C$)

T_m (°C)	t_{ext} (h)	V_{TES} (m^3)	T_{up} (°C)	T_{low} (°C)	ΔE_{ext} (MWh)	ΔE_{ext} (MJ)	e_{ext} (%)	e_{day} (%)	ΔT_{source} (°C)
30	8.7	1528	26.0	29.2	9.0	32,400	2.06	0.73	5.4
28	9.2	2020	24.7	29.2	12.7	45,720	2.73	1.03	7.0
27	—	—	—	—	—	—	—	—	—
21	8.9	1780	15.5	20.2	14.9	53,640	3.25	1.18	8.8

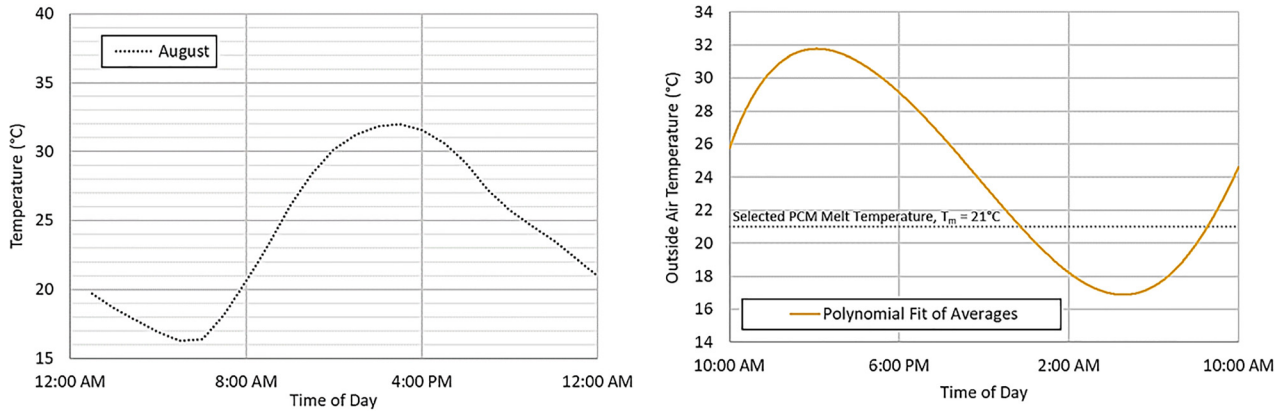

Fig. 12 (left) Average hourly Reno, NV temperature data for August, averaged from 2013 to 2017 and (right) approximate polynomial curve for outside air temperature throughout an average August day in Reno, NV

To find the payback period of each of the investments of interest using only the revenue directly resulting from the implementation of the TES and external heat exchanger subsystems, Eq. (15) was used. The results of this cost analysis are shown in Table 5.

$$t_{payback} = C_{inv}/P_{annual} \tag{15}$$

The values in Table 5 shown in the last three rows correspond to electricity sold at a premium rate. Project collaborators from the University of Cincinnati have advised that the excess energy generation provided by the implementation of the TES and external heat exchanger subsystem will be generated at times of peak power demands and should be priced accordingly. Therefore, the peak-demand price was estimated to be four times that of the nominal residential cost of electricity. Adjusting for this premium electricity price in the three PCM melt temperature cases of interest, the excess daily revenue for each of these cases increased significantly, and, correspondingly, their payback period decreased significantly as well. Thus, investments ranging from $12.4 million to $17.3 million for the three PCM melt temperature cases had payback periods ranging from 21.3 to 25.5 years. It should be noted that the cost of the PCM makes up approximately 15% of the overall TES investment, so if the cost to make the heat exchange structure within the TES could be lowered through increased efficiency of manufacturing processes, the payback periods would be reduced accordingly.

Table 5 Summary of TES properties and cost analysis

Location	Las Vegas, NV	Las Vegas, NV	Reno, NV
PCM melt temperature	30 °C	28 °C	21 °C
TES volume	3000 m^3	4200 m^3	3500 m^3
TES storage capacity	814,410 MJ	1,136,600 MJ	948,200 MJ
TES principal investment	$12.4 million	$17.3 million	$14.4 million
Electricity cost	$0.44/kWh	$0.44/kWh	$0.36/kWh
TES excess revenue	$486,000/year	$686,000/year	$667,000/year
Payback time	25.5 years	25.2 years	21.6 years

Conclusions

The goal of this study was to use Helmns and Carey's model of TES in conjunction with a subsystem that employs cool storage to precool the air flow for a power plant air-cooled condenser during peak daytime temperatures. This model was used to explore the effects of varying PCM melt temperature and the energy storage and extraction control settings for the system. The subsystem model was also computationally linked to a model of Rankine cycle power plant performance to predict how much additional power the plant could generate as a result of the asynchronous cooling augmentation provided by this subsystem.

The results suggest that for a full-sized power plant with a nominal capacity of 50 MW, the kWh output of the plant can be increased by up to 3.25% during the extraction period, depending on parameter choices, including PCM melt temperature, TES volume and extraction time, temperature threshold, and location. Overall, trends showed that the implementation of the TES and external heat exchanger subsystem into a Rankine power plant with an air-cooled steam condenser provided significant improvement to its overall production capabilities.

For the three different cases with optimized conditions, cost analyses were performed, and it was estimated that the TES and external heat exchanger subsystem has the potential to provide additional revenue ranging from $486,000 to $686,000 per year depending on location, TES storage capacity, and electricity cost. With initial investments for these TES structures ranging from $12.4 to $17.3 million, the payback periods were estimated to range from 21.3 to 25.5 years, making the TES and external heat exchanger subsystem a decent investment.

Funding Data

- Advanced Research in Dry cooling (ARID) Program of the Advanced Research Projects Agency—Energy (ARPA-E) (No. DE-AR0000577; Funder ID: 10.13039/100006133).

Nomenclature

A_c = cross-sectional area of flow passage channel
c_{pw} = working fluid specific heat; may be written as $c_{p,open}$ or $c_{p,closed}$

$\bar{c}_{pe}$ = effective specific heat of TES differential element
C_{elec} = cost of electricity
C_{inv} = cost to be paid off for TES investment
C_{TES} = cost of initial TES investment
dz = length of TES differential element
e_{day} = percent increase in energy produced in power plant during 24-hour period due to implementation of TES and external heat exchanger subsystem
e_{ext} = percent increase in energy produced in power plant during precooling window due to implementation of TES and external heat exchanger subsystem
E_{day} = energy produced in power plant throughout the rest of the day after precooling phase
E_{ext} = energy produced in power plant with TES and external heat exchanger subsystem during precooling phase
$E_{no\ ext}$ = energy produced in power plant without TES and external heat exchanger subsystem during what would have been precooling phase
E_{TES} = storage capacity of TES
f = fraction of year TES is considered operable
h_{ls} = latent heat of fusion of PCM
L = length of flow passage
$\dot{m}_{closed}$ = working fluid closed-loop mass flow rate through TES; may be written as $\dot{m}$ext or $\dot{m}$char
$\dot{m}_{open}$ = working fluid open-loop mass flow rate through external HX; may be written as $\dot{m}$source or $\dot{m}$sink
$\dot{Q}$ = heat transfer rate in the external HX; may be written as $\dot{Q}$source or $\dot{Q}$sink
$\dot{Q}_{sc}$ = heat transfer rate in steam condenser of Rankine cycle power plant
r = interest rate for TES investment
s_w = wetted perimeter of flow passage
t = time variable
t_{ext} = length of extraction/precooling process
T_{amb} = outside ambient air temperature
T_{closed} = TES closed loop working fluid temperature; may be written as T_{ext} or T_{char}
T_e = TES device matrix element temperature
T_m = melting temperature of PCM
T_{open} = external HX open-loop working fluid temperature; may be written as T_{source} or T_{sink}
T_{thresh} = temperature threshold for entering and exiting storage processes; may be written as T_{up} or T_{low}
U_{closed} = overall heat transfer coefficient between bulk working fluid and PCM matrix element; may be written as U_{ext} or U_{char}
V_{TES} = TES total volume
$\dot{W}$ = assumed constant power production of Rankine cycle power plant
$\dot{W}_{var}$ = variable power production of Rankine cycle power plant
x_e = melt fraction of PCM in matrix element
ΔE_{ext} = difference in energy produced in power plant with and without precooling process
ΔT_{source} = difference between open-loop inlet and outlet temperatures of the precooler external heat exchanger (HX) at the peak ambient temperatureε_{hx}
= effectiveness of external HX; may be written as ε_{source} or ε_{sink}
ε_{TES} = effectiveness of TES; may be written as ε_{ext} or ε_{char}
η_{cyc} = assumed constant thermal efficiency of Rankine power plant
$\eta_{cyc,var}$ = variable thermal efficiency of Rankine power plant
ν' = PCM matrix volume per unit flow length
ρ_{PCM} = density of PCM averaged between liquid and solid phases
ρ_w = working fluid density; may be written as ρ_{open} or ρ_{closed}
$\bar{\rho}_e$ = effective density of TES differential element

References

[1] EPRI, 2010, "The Other Foot Print," EPRI J., (2), p. 11.
[2] Farid, M. M., Khudhair, A. M., Razack, S. A. K., and Al-Hallaj, S., 2004, "A Review on Phase Change Energy Storage: Materials and Applications," Energy Convers. Manage., **45**(9–10), pp. 1597–1615.
[3] Sabihuddin, S., Kiprakis, A. E., Mueller, M., and Numerical, "A., and 2014, "Graphical Review of Energy Storage Technologies," Energies, **8**(1), pp. 172–216.
[4] Lindsay, B. B., and Andrepont, J. S., 2019, "Evolution of Thermal Energy Storage for Cooling Applications," AHSRAE, **61**(10), pp. 42–59.
[5] El-Dessouky, H., and Al-Juwayhel, F., 1997, "Effectiveness of a Thermal Energy Storage System Using Phase-Change Materials," Energy Convers. Manage., **38**(6), pp. 601–617.
[6] Ismail, K., and Goncalves, M., 1999, "Thermal Performance of a PCM Storage Unit," Energy Convers. Manage., **40**(2), pp. 115–138.
[7] Alkilani, M. M., Sopian, K., Mat, S., and Alghoul, M. A., 2009, "Output Air Temperature Prediction in a Solar Air Heater Integrated With Phase Change Material," Eur. J. Sci. Res., **27**(3), pp. 334–341.
[8] Vakilaltojjar, S. M., and Saman, W., 2001, "Analysis and Modelling of a Phase Change Storage System," Appl. Therm. Eng., **21**(3), pp. 249–263.
[9] Helmns, A., and Carey, V. P., 2018, "Multi-Scale Transient Modeling of Latent Energy Storage for Asynchronous Cooling," ASME J. Therm. Sci. Eng. Appl., **10**(5), p. 051004.
[10] Helmns, A., and Carey, V. P., 2017, "Modeling of Intramatrix Heat Transfer in Thermal Energy Storage for Asynchronous Cooling," ASME Paper No. HT2017-4870.
[11] Theroff, Z., Helmns, M. A., and Carey, V. P., 2018, "Exploration of Variable Conductance Effects During Input and Extraction of Heat From Phase Change Thermal Storage," ASME Paper No. IMECE2018-88078.
[12] Shamberger, P. J., and Reid, T., 2012, "Thermophysical Properties of Lithium Nitrate Trihydrate From (253 to 353) k," J. Chem. Eng. Data, **57**(5), pp. 1404–1411.
[13] NCEI, 2017, "Data Tools: Local Climatological Data (LCD)," NOAA National Centers for Environmental Information, NCEI, accessed Apr. 3, 2020, https://www.ncdc.noaa.gov/cdo-web/datatools/lcd
[14] Nevada Power Company, 2017, "NV Energy Electric Rate Schedules for Residential Customers," Nevada Power Company, Las Vegas, NV, accessed Apr. 1, 2018, https://www.nvenergy.com/publish/content/dam/nvenergy/brochures_arch/about-nvenergy/rates-regulatory/np_res_rate.pdf
[15] Sierra Pacific Power Company, 2018, "NV Energy Electric Rate Schedules for Residential Customers," Sierra Pacific Power Company, Reno, NV, accessed Apr. 1, 2018, https://www.nvenergy.com/publish/content/dam/nvenergy/brochures_arch/about-nvenergy/rates-regulatory/spp_nv_resrates.pdf